A&A manuscript no.
(will be inserted by hand later)

Your thesaurus codes are:
06 (08.16.4 08.02.5 08.05.3 08.12.1)

ASTRONOMY AND ASTROPHYSICS
May 24, 2000

The Henize sample of S stars

III. Uncovering the binary intruders *

S. Van Eck[1,2] **and A. Jorissen**[1] **

[1] Institut d'Astronomie et d'Astrophysique (IAA), Université Libre de Bruxelles, C.P.226, Boulevard du Triomphe, B-1050 Bruxelles, Belgium
[2] European Southern Observatory, Karl-Schwarzschild Strasse 2, D-85748 Garching bei München, Germany

Received date; accepted date

Abstract. The properties of S stars are investigated thanks to a large observing program devoted to the well-defined Henize sample (205 S stars south of $\delta = -25°$ and brighter than $R = 10.5$, covering all galactic latitudes), in order to derive the respective properties of the intrinsic S stars (genuine thermally-pulsing AGB stars) and of the extrinsic S stars (post mass-transfer binaries).

The stellar sample is first cleaned from a few stars misclassified as S thanks to UBV Geneva photometry and low-resolution spectroscopy. These low-resolution spectra also allow to successfully distinguish subclasses within the S star family. Dedicated Geneva photometry and high-resolution spectroscopy have led to the discovery of two symbiotic S stars.

The more stringent difference between extrinsic and intrinsic stars is their technetium content, but several other observational parameters are shown to be efficient to some extent in segregating intrinsic S stars from their extrinsic masqueraders (UBV, $JHKL$ and IRAS photometry, radial-velocity standard deviation, shape of the CORAVEL cross-correlation dip, combination of band strength indices derived from low-resolution spectra). Multivariate classification has been performed on the Henize data sample in order to guarantee a classification as objective as possible and handling at the same time a large number of parameters. The resulting clusters separate efficiently extrinsic and intrinsic S stars, allowing to derive the respective properties of these two distinct stellar classes. The population difference between intrinsic and extrinsic S stars is for the first time clearly demonstrated, since intrinsic S stars are far more concentrated towards the galactic plane than extrinsic S stars ($z_{\rm int} = 200 \pm 100$ pc and $z_{\rm ext} = 600 \pm 100$ pc), and are therefore believed to belong to a younger, more massive population. The frequency of extrinsic and intrinsic S stars in the magnitude-limited Henize sample amounts to 33% and 67%, respectively. In a volume-limited sample, this proportion is subject to large uncertainties mainly because of uncertain luminosities. There are probably as many as 40% extrinsic stars among S stars in a volume-limited sample.

Key words: Stars: late-type – Stars: AGB and post-AGB – Stars: evolution – binaries: symbiotic

1. Introduction

S stars have temperatures similar to those of M-type giants, but their characteristic spectral features are ZrO bands. TiO bands are generally present as well, except in the so-called 'pure' S stars. They are in fact truly enriched in carbon and heavy elements (e.g. Smith & Lambert 1990, Vanture et al. 1991) produced by the s-process (e.g. Arnould 1991). Therefore they are commonly believed to be located on the *thermally-pulsing asymptotic giant branch* (TPAGB), where the repeated occurrence of thermal pulses and third dredge-up episodes permits carbon and s-process elements to be synthesized and brought to the stellar surface.

However, Iben & Renzini (1983) were the first to question this picture after the discovery of technetium-poor (Tc-poor) S stars (Little-Marenin & Little 1979; Little et al. 1987). Technetium is a s-process element with no stable isotopes, and the laboratory half-life of ^{99}Tc, the isotope produced by the s-process, is 2.13×10^5 y, of the order of the TPAGB duration. Therefore if all S stars were located on the TPAGB, they should all exhibit technetium, unless third dredge-up episodes are so widely spaced in time that technetium has time to decay below its spectroscopic detection threshold between two dredge-up episodes (Busso et al. 1992).

A more likely explanation for the origin of Tc-poor S stars arose with the discovery of their evolutionary link

Send offprint requests to: S. Van Eck, svaneck@eso.org
* Based on observations carried out at the European Southern Observatory (ESO, La Silla, Chile) and at the Swiss 70 cm telescope (La Silla, Chile)
** Research Associate, National Fund for Scientific Research (FNRS), Belgium
Correspondence to: S. Van Eck

with barium stars. Barium stars are G-K giants with enhanced s-process elements, but their too low luminosities forbid them from being located on the TPAGB (Scalo 1976). All have been proven to be binaries (e.g. McClure & Woodsworth 1990; Jorissen et al. 1998) with white dwarf companions. Hence, their chemical peculiarities are believed to originate in a former mass-transfer episode across the binary system: while still on the main sequence, the progenitor of the present barium star accreted s-process-rich matter from its companion, a mass-losing TPAGB star at that time. Hence barium stars are giant stars enriched in s-process elements, though they have not produced these elements themselves.

As barium stars cool down while evolving on the red giant branch (or on the early-AGB), ZrO bands become detectable in their spectra and they show off as S stars without Tc, because Tc had enough time to decay since it was produced by the companion. Hence Tc-poor S stars (also called *extrinsic*, as opposed to the *intrinsic*, Tc-rich TPAGB S stars) can be easily explained as cool descendants of barium stars in the framework of a binary scenario.

This binary scenario for Tc-poor S stars is expected to imprint various signatures. The present work aims at testing this scenario by studying an homogeneous, well-defined sample of S stars, in order to separate extrinsic from intrinsic S stars and to derive the respective properties of these two distinct stellar families – until now widely confused. As will be shown in this paper, a closer look at S stars indeed reveals a clear dichotomy, not only in terms of presence or absence of Tc, but also of various other features. Yet it is of key importance to distinguish the TPAGB stars from the extrinsic (less evolved) masqueraders, because the latter will otherwise introduce strong biases. For instance, the third dredge-up luminosity threshold, commonly derived as the transition luminosity between M and S stars, may be totally in error if extrinsic S stars have not been removed from the studied sample. In the same vein, the ratio of S stars to M or C stars must be corrected for the presence of extrinsic stars (possibly among C stars as well), when trying to deduce from this ratio the respective durations of the EAGB and TPAGB.

The Henize[1] sample of 205 S stars (as listed in Stephenson 1984) is supposed to comprise all the S stars south of $\delta = -25°$ and brighter than $R = 10.5$. Its completeness will be discussed in more details in Sect. 9.3. Its main advantage, contrarily to many other S-star surveys, is that it covers all galactic latitudes instead of being limited to the galactic plane. A large-scale observing program has thus been devoted to the Henize sample at the European Southern Observatory (La Silla), resulting in (i) a five-year radial-velocity monitoring, with 4-5 measurements per star, in order to detect binarity, (ii) Tc spectra for 70 stars, in order to infer the technetium content, (iii) 158 low-resolution spectra in order to detect misclassified stars. A photometric survey of the Henize sample in the Geneva photometric system was also conducted on the 70cm Swiss telescope at La Silla. *JHKL* photometry taken at the South African Astronomical Observatory (SAAO) is also available, as well as IRAS infrared fluxes.

The technetium data for the Henize sample have been discussed in Van Eck & Jorissen (1999, hereafter referred to as Paper I). The material relating to radial velocities, photometry and low-resolution spectroscopy is presented in Van Eck et al. 2000 (Paper II). The present paper is devoted to a global analysis of these data. After a discussion of the radial-velocity data of the Henize S stars (Sect. 2), their Geneva photometry is examined (Sect. 3), as well as their IRAS photometry (Sect. 4). Spectral indices computed from the low-resolution spectra are discussed in Sect. 5. Multivariate classification is performed on the whole material collected on the Henize sample in Sect. 6, and allows to distinguish efficiently extrinsic from intrinsic S stars. Sect. 7 then confirms the binary nature of extrinsic S stars, and the galactic distributions of both kinds of S stars are examined in Sect. 8. Finally, the frequency of extrinsic and intrinsic S stars is estimated in Sect. 9.

2. Radial velocities of S stars

2.1. The CORAVEL parameter Sb

CORAVEL (Baranne et al. 1979) measures the radial velocity of a star by cross-correlating its spectrum with a mask reproducing about 1500 lines of neutral and ionized iron-group species from the spectrum of Arcturus (K1-2 III). The minimum of the resulting cross-correlation dip (cc-dip) yields the radial velocity of the star. In fact, useful additional information may be derived from the cc-dip: in particular, the parameter *Sb*, defined as the width of the cc-dip corrected from the instrumental profile (see Paper II), is related to the average stellar line width. In relatively unevolved giants (like G, K, barium stars or Tc-poor S stars), the cc-dip is narrow, strongly contrasted and has a non-variable shape. On the contrary, the cc-dip of Mira stars is wide, shallow and strongly variable with time (see Fig. 1).

There are probably several reasons for the distorted cc-dips of Mira stars (Barbier et al. 1988). First, the atmosphere of a Mira star is characterized by a complex velocity field; the cc-dip of a Mira star is thus a combination of several (variable) cc-dips, each dip corresponding to a layer moving with a given velocity (Udry et al. 1998; Wallerstein 1985). Hence the width of the resulting cc-dip is larger and more variable than if the star had a stable atmosphere. This link between *Sb* and the pulsational characteristics

[1] In the following the Henize S stars are referred to as "Hen *nnn*"; this notation corresponds to "Henun *nnn*" in Stephenson (1984), though these S stars are referred to as "Hen 4-*nnn*" in the Simbad database

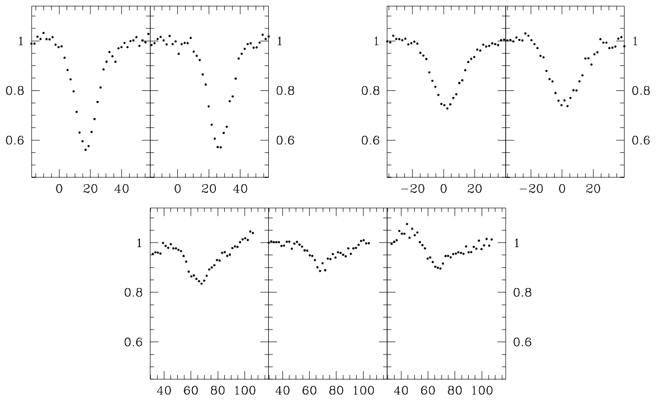

Fig. 1. CORAVEL cross-correlation dips for the extrinsic, Tc-poor S star Hen 2 (upper-left panels), for the intrinsic, Tc-rich S star Hen 97 (upper-right panels) and for the (intrinsic) Mira S star Hen 32 = SU Pup (lower panels). The different panels for a given star correspond to different observing dates. Abscissae are graduated in km s^{-1}. The mean values of the *Sb* parameter are 4.2 km s^{-1}, 7.7 km s^{-1} and 8.5 km s^{-1} for Hen 2, Hen 97 and Hen 32, respectively

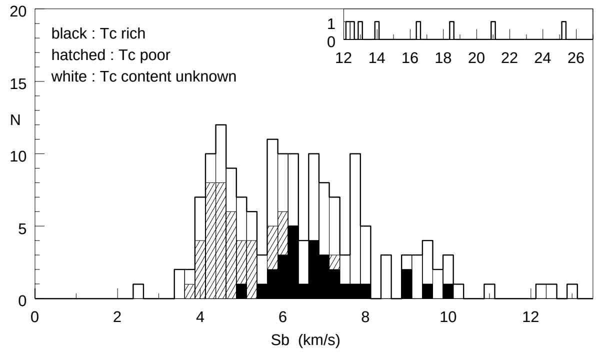

Fig. 2. Histogram of the cc-dip widths (expressed in terms of *Sb*, see text) for the Henize S stars. The inset represents the large *Sb* tail of the histogram, comprising mainly Mira S stars or SC stars

of the atmosphere is further confirmed by the strong trend of increasing *Sb* with increasing radial-velocity jitter (see Fig. 1 of Jorissen et al. 1998).

Second, the CORAVEL mask is optimized for Arcturus-type (K1-2) giants. In cooler stars like S stars, the relative line intensities are different, and additional molecular lines are encountered: such inadequacies of the mask with respect to the stellar spectrum are in part responsible for the shallower cc-dips of S stars (Alvarez, priv. comm.). The broadening of spectral lines due to the increase of macroturbulence with luminosity – previously believed to be the main cause of the cc-dip widening (Jorissen et al. 1998) – probably plays only a minor role in shaping the cc-dip.

Since intrinsic S stars are by definition on the TPAGB, they are expected to be on average more evolved than extrinsic, mass-transfer S stars; their *Sb* parameter is consequently expected to be larger. This is indeed the case, as shown in Fig. 2: the distribution of the *Sb* parameter is clearly bimodal, the first peak ($Sb < 5.5$ km s^{-1}) comprising mostly Tc-poor stars, and the second one ($Sb \geq 5.5$ km s^{-1}) mainly Tc-rich stars. The lack of systems around $Sb \sim 5.5$ km s^{-1} is not dependent on the adopted binning of the data, but reveals the real bimodal nature of the distribution. Hence the *Sb* parameter appears to be a useful tool to distinguish, with a good statistical efficiency, intrinsic from extrinsic S stars, when no information on their technetium content is available.

2.2. Binarity in the Henize sample

The intrinsic/extrinsic paradigm requires Tc-poor S stars to belong to binary systems. Hence, the radial-velocity standard deviation is expected to be larger for Tc-poor S stars than for Tc-rich S stars. This is indeed the case, since the mean value of the radial-velocity standard deviation is $\langle\sigma(V_{\rm r})\rangle = 3.2 \pm 2.4$ (rms) km s^{-1} for Tc-poor S stars, as compared to 1.3 ± 0.7 (rms) km s^{-1} for Tc-rich S stars. This point will be further examined in Sect. 7.

The orbital parameters that could be derived for 8 Henize S stars (see Paper II) are typical of the few orbits already known for extrinsic S stars (Jorissen et al. 1998). The Henize sample contains in fact the S star with the second shortest orbital period known (Hen 108, P = 197 d). Such a short orbital period sets strong constraints on the radius of the S star that has to fit inside its Roche lobe. Adopting 0.6 M$_\odot$ for the mass of the white dwarf companion, the radius of the Roche lobe around the S star is $\sim$ 50 R$_\odot$, with little sensitivity to its adopted mass (taken within the reasonable limits 1-4 M$_\odot$). Given an effective temperature of $\sim$ 3700 K as derived from the $V-K$ colour index and the calibration of Ridgway et al. (1980), and an absolute bolometric magnitude in the range $-2 \leq M_{\rm bol} \leq -3.5$ (Van Eck et al. 1998), the resulting radius lies in the range 54 R$_\odot$ to 109 R$_\odot$. Hence this star must be extremely close to filling its Roche lobe, or even currently undergoes a stable Roche-lobe overflow. In fact, this star could be expected to exhibit symbiotic activity; however a high-resolution spectrum of this star around H$_\alpha$ taken on February 23, 1998 (Van Eck & Jorissen 2000, Paper IV) reveals no emission line whatsoever. Moreover, Hen 108 does not exhibit abnormally blue colours in the Geneva system as it is the case for the other symbiotic S stars discovered so far (Sect. 3.2).

In fact, the only S star known to have a shorter period than Hen 108 is HD 121447 (P = 186 d, Jorissen et al. 1998), an early S star (S0, Keenan 1950), also known as the coolest barium star (K7III Ba5, Lü 1991). This system was found to be an ellipsoidal variable (Jorissen et al. 1995). Due to its similarity with HD 121447, Hen 108 may be suspected to be an ellipsoidal variable as well; unfor-

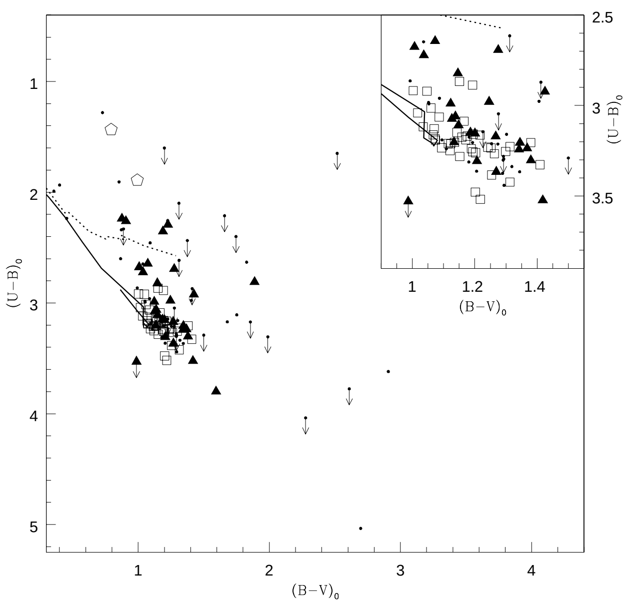

Fig. 3. Dereddened colour-colour diagram, in the Geneva photometric system, of the Henize S stars. A zoom is presented in the upper-right inset. Tc-rich S stars are represented by black triangles, Tc-poor S stars by open squares, stars for which no Tc information is available by dots, and the two (Tc-poor) symbiotic S stars by open pentagons. The stars that have only upper limits on their U flux (i.e., stars with some of their U measurements falling above the rejection threshold $U = 16.5$; see Paper II) are flagged with an arrow . The solid and dotted lines are the normal giant and dwarf sequences, respectively, from Grenon (1978)

tunately the available photometric data are too scarce to check this hypothesis.

3. Geneva photometry

3.1. Colour-colour diagram

In the $(U-B, B-V)_0$ colour-colour diagram (Fig. 3), Tc-poor stars tend to cluster close to the normal giant sequence. The lack of extrinsic S stars with very blue and variable colours, that would be the signature of a nebular continuum as in symbiotic stars, will be further commented in Sect 3.2. Note also that information on the technetium content is only available for the bluest stars, since the technetium lines used in this study are located in the violet around 4260Å.

Intrinsic S stars are known to be generally redder than extrinsic S stars (Van Eck et al. 1998). This property is not clearly visible on Fig. 3, mainly because of a strong observational bias: the reddest S stars were generally too faint in the U filter and do not therefore appear on Fig. 3, except for some relatively bright stars. In that respect it must be noted that the stars with $(B-V)_0 > 2$ are generally pure S stars (i.e., exhibiting only ZrO bands and no TiO) or SC stars; this point will be further discussed in Sect. 5.3. The extremely red star at $(U-B)_0 = 5.0, (B-V)_0 = 2.7$ is the bright prototype SC star Hen 135 = UY Cen.

On the contrary, many blue Miras are found where symbiotic S stars were expected [e.g., Hen 56: $(U-B)_0 = 1.6$, $(B-V)_0 = 1.2$, $\sigma(U) = 0.3$, or Hen 125: $(U-B)_0 = 2.3$, $(B-V)_0 = 0.9$, $\sigma(U) = 0.2$]. The blue colours of some Miras were already noted by Nakagiri & Yamashita (1979). The location of Miras in their $(U-B, B-V)$ diagram (their Figs. 17, 18 and 19) is very similar to the location of Henize blue Miras in Fig. 3. Nakagiri & Yamashita found that Miras describe loops in this part of the colour-colour diagram over a complete cycle. A similar behaviour is observed for prototypical Miras present in the Geneva photometric catalogue (e.g. R Hor, R Cnc or o Cet), and is related to the passage of the shock wave associated with pulsations through the photosphere [see Gillet et al. (1989) for a discussion of a similar behaviour among RR Lyrae variables].

Because of the blue excursions of many Miras from the Henize sample, no clear distinction is observed between intrinsic and extrinsic S stars on the basis of the UBV colour indices. However, the blue Miras exhibit a much larger variability than do extrinsic S stars (at least the non-symbiotic extrinsic): hence it is often possible to distinguish intrinsic from extrinsic S stars by combining colour indices and photometric variability information. This will be done in Sect. 6.

3.2. Symbiotic stars

Since all extrinsic S stars belong to binary systems, one could expect to see photometric signatures induced by the presence of their compact (white dwarf) companion, like in symbiotic systems. Indeed, symbiotic stars are interacting binaries in which the cool component is a late-type giant interacting with a compact companion (in most cases a white dwarf, sometimes a main-sequence or a neutron star). The mass loss of the giant star feeds a nebula which engulfs the components and gives rise to a veiling blue continuum and intense superposed nebular emission lines.

In fact, the U filter ($\sim 3050-3850$Å), and, to a much lesser extent, the B filter ($\sim 3650-5150$Å), are sensitive to the blue flux excess of symbiotic stars; as a consequence, symbiotic stars occupy extremely peculiar and variable positions in the $(U-B, B-V)_0$ colour-colour diagram. Excursions of symbiotic stars towards the blue in that colour-colour diagram were already noticed by Arkhipova & Noskova (1985), and are seen as well for prototypical symbiotic stars monitored in the Geneva photometric system (especially R Aqr and T CrB, and to a lesser extent, BL Tel, Z And and AG Peg).

Only two extrinsic S stars of the Henize sample exhibit abnormally blue colours in Fig. 3: Hen 18 and Hen 121, represented by open pentagons on Fig.3 (the other blue stars are most probably blue Miras, i.e. intrinsic stars; indeed, their photometric variability and CORAVEL cc-dips are more typical of Miras than of symbiotics). The emission lines characteristic of symbiotic stars have been searched for in these two stars, as well as in 29 other "abnormally blue" stars of the Henize sample, with high-resolution spectroscopy. Both Hen 18 and 121 show a definite, though weak, symbiotic activity, in that they exhibit the very broad H_α emission (basewidth > 300km s^{-1}, see Paper IV) with blue-shifted absorption typical of symbiotics, but no other clear emission line.

Though the symbiotic family comprises over 200 objects, only 3 symbiotic S stars were known to date (Jorissen 1997; Mürset & Schmid 1999); Hen 18 and 121 constitute two new discoveries in this restricted family and, like the other symbiotic S stars, their symbiotic activity is moderate. These two stars are found to be binaries and their orbital periods ($P = 764$ d for Hen 121, $P > 1800$ d for Hen 18, Paper II) appear typical of those of normal extrinsic S stars.

The 29 additional "blue" S stars also examined for symbiotic activity did not exhibit such remarkable symbiotic features at the epoch of observation. It is thus noteworthy that only the two stars Hen 18 and 121, out of the 29 blue Henize stars spectroscopically examined (and possibly out of the 172 stars having Geneva photometry) exhibit a clear symbiotic signature at the epoch of observation. This fact underlines that the key factor triggering symbiotic activity is not yet fully understood: it is not sufficient to have a red giant and a white dwarf in a binary system with periods typically in the range 200-10 000 d to develop symbiotic activity; some additional physical ingredients (involving metallicity, luminosity, masses of the components, mass loss, presence and properties of a disk fed by an enhanced mass loss?) are clearly required.

4. IRAS photometry

Intrinsic and extrinsic S stars have been shown to segregate well in the $(K-[12], K-[25])$ diagram (Groenewegen 1993; Jorissen et al. 1993). Here the colour index $K-[i]$ is defined as $K-[i] = K + 2.5 \times log[F(i)/F_0(i)]$, where $F(i)$ is the (non colour-corrected) flux in the i band from the IRAS Point Source Catalogue, $F_0(12\mu\text{m}) = 28.3$ Jy, and $F_0(25\mu\text{m}) = 6.73$ Jy. Indeed, Fig. 4 confirms this nice segregation among the S stars of the Henize sample. More precisely, Henize extrinsic S stars always fulfill the conditions $K-[12] < 0.9$ and $K-[25] < 0.9$. The $([12]-[25], [25]-[60])$ colour-colour diagram is less useful, because good quality $[12]-[25]$ and $[25]-[60]$ colours are only available for 27 stars, among which only 7 are known to be Tc-rich and 1 is Tc-poor.

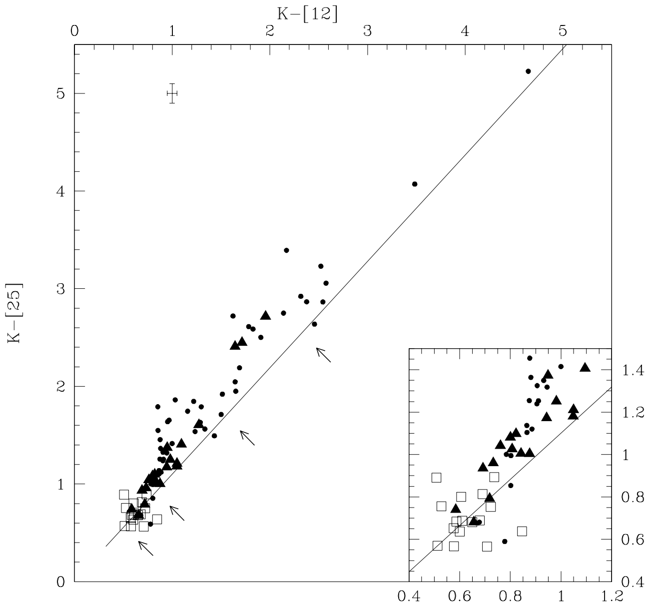

Fig. 4. The $(K-[12], K-[25])$ colour-colour diagram of Henize S stars. Open squares stand for Tc-poor S stars, filled triangles for Tc-rich S stars and black dots for S stars with unknown technetium content. Only the good-quality (flag=3) IRAS fluxes have been used. The error bars correspond to a typical uncertainty of 5 and 10% on the 12 and 25 μm fluxes, respectively. The solid line represents black body colours, with arrows corresponding to temperatures of 4000, 3000, 2000 and 1500 K (from lower left to upper right)

5. Low-resolution spectroscopy

5.1. Misclassified stars

Low-resolution spectra, covering the spectral range 4400-8200Å, were obtained with the aim of detecting possible non-S stars polluting the Henize sample. In fact the complete Henize sample of 205 S stars could not be observed because of the limited observing time allocated.

For the 158 stars with available low-resolution spectra, a system of band-strength indices has been constructed that indicates the strength of a specific band (or line) with respect to a nearby pseudo-continuum (Paper II). In fact such band-strength indices allow to efficiently unmask misclassified S stars, as shown on Fig. 5. Indeed, as far as non-S stars are concerned, K and M giants all have $I_{\rm ZrO} < 0.1$ as expected, as well as the M dwarfs and supergiants. Furthermore, their temperature type nicely increases with the TiO index. On the contrary, virtually all Henize stars have $I_{\rm ZrO} > 0.1$, as well as the three additional well-known S stars for which spectra were also obtained (HD 35155, HD 49368, GG Pup). The only exceptions are Hen 4, 22, 58, 127 and 154, which have $I_{\rm ZrO} < 0.1$.

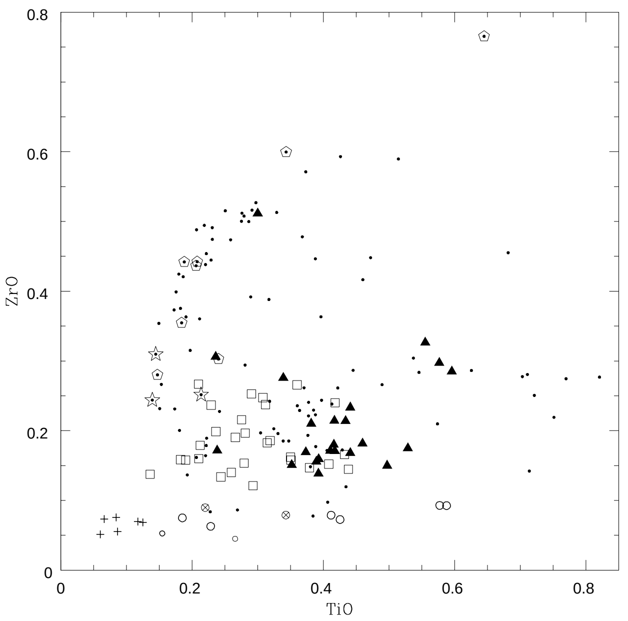

Fig. 5. ZrO index versus TiO index, as derived from low-resolution spectra with $S/N \geq 60$. Symbols are as follows: plusses for late G or K stars, open circles for M giants, small open circles for M dwarfs, crossed circles for M supergiants, open squares for Tc-poor S stars, filled triangles for Tc-rich S stars, dots for stars with unknown Tc content, open pentagons for late S stars also belonging to the Westerlund-Olander sample, open star symbols for previously-known SC stars.

Hen 22 and 154 have already been recognised as a late G (~G8) giant and a mid-K (~K3-5) giant, respectively, on the basis of the very same low-resolution spectra (see Paper I). In Fig. 5, they are the two stars with $I_{\rm ZrO} \approx 0.05$ and $I_{\rm TiO} < 0.1$.

Hen 4 and Hen 127 (both with $I_{\rm ZrO} = 0.08$) have definite TiO bands but barely visible (possibly uncertain) ZrO bands. In fact, Hen 58 ($I_{\rm ZrO} = 0.09$) and Hen 40 ($I_{\rm ZrO} = 0.12$) somehow fall in the same category, while Hen 67, having $I_{\rm ZrO} = 0.10$, is an S star (i.e. has well visible ZrO bands). Hence the boundary between M and S stars falls somewhere in the range $0.09 \leq I_{\rm ZrO} \leq 0.12$, depending on temperature. The evidence for Hen 4, 40, 58 and 127 being misclassified as S stars is however too weak to justify their elimination from the final sample considered for analysis.

Chen & Kwok (1993) mention that Hen 124 (= GCSS 447 = GCGSS 798) "is known to have been misclassified and is not an S star" without any other justification. However on the basis of our low-resolution spectra we confirm that Hen 124 is not misclassified and is indeed an S star.

Finally, Stephenson has excluded Hen 169 from the second edition of its Catalogue of S stars (Stephenson 1984), for this star was reclassified as carbon in the Ph.D. thesis of Rybski (1972). However our four CORAVEL radial-velocity measurements show a very narrow (*Sb* = 3.5 km s^{-1}), deep (PR=0.44) and non-variable (i.e., without jitter) cc-dip more typical of extrinsic S stars rather than of carbon stars. Given the lack of further information on this star, it has been kept in our sample of S stars.

To conclude with, the number of misclassified stars in the total sample is most probably very low, since out of the 158 Henize S stars with a low-resolution spectrum available, only two (Henize 22 and 154) turn out to be clearly non-S stars.

5.2. ZrO and TiO band strengths of S stars

The 158 spectra obtained not only allow to detect misclassified stars, but also to distinguish subclasses within the S family according to the strength of TiO, ZrO, LaO bands and sodium D lines.

The plane of ZrO and TiO indices displayed in Fig. 5 exhibits a complex structure. Although Tc-rich and Tc-poor S stars somehow segregate on the lower branch (i.e., in the region $I_{\rm ZrO} \lesssim 0.3$), there is a second, curved branch extending upwards, which contains mainly SC stars and late, nearly pure or pure S stars with LaO bands.

The band strengths in S stars depend upon many parameters (temperature, C/O ratio, s-process abundances), and the interpretation of the trends observed on Fig. 5 must therefore rely on detailed molecular-equilibrium calculations, as provided by e.g., Scalo & Ross (1976) and Piccirillo (1980).

In fact, Fig. 5 is a good illustration of the difficulty of classifying S stars solely on the basis of their ZrO and TiO band strengths. This was already recognised by Keenan & McNeil (1976) and Ake (1979), who replaced the old Keenan (1954) classification scheme (temperature and abundance classes defined by combining the ZrO and TiO band strengths) by a classification where the TiO and ZrO indices are listed separately. Even then, additional information is needed (as provided, e.g., by the Na D line index described in Sect. 5.3), because SC stars fall close to extrinsic S stars in Fig. 5. This difficulty mainly arises because as a star evolves along the AGB, its temperature is expected to decrease while its C/O ratio is expected to increase, but these two factors have opposite effects on the main band strengths.

Fig. 5 may actually be described in terms of a counter-clockwise loop of increasing C/O ratio. In fact, the classification scheme of Ake (1979), based on Piccirillo's results, uses the ZrO, TiO and YO band strengths to classify S stars in six classes of C/O ratios. Ake's classification implies that, when C/O evolves from 0.9 to unity, S stars describe a counter-clockwise loop in Fig. 5, from the right side of the lower branch ($I_{\rm ZrO}$=0.2, $I_{\rm TiO}$=0.5) up to the right side of the upper branch ($I_{\rm ZrO}$=0.5, $I_{\rm TiO}$=0.3) and down this branch to $I_{\rm ZrO}$=0.2, $I_{\rm TiO}$=0.2. The fact that C/O increases downward along the upper branch is confirmed by the following observations: (i) the higher regions of the upper branch are mostly populated by late and nearly pure S stars from the Westerlund-Olander survey (Westerlund & Olander 1978), a survey based on the LaO band strength. Strong LaO bands appear in cool stars with C/O ratios close to unity (Piccirillo 1980); (ii) SC stars (which are characterized by a C/O ratio of almost unity) are located at the lower left end of the upper branch ($I_{\rm TiO} \sim 0.15, I_{\rm ZrO} \sim 0.25$).

Nevertheless, Piccirillo (1980) also stressed that the increase in C/O alone cannot account for the increasing strength of ZrO bands in the M-MS-S sequence for stars warmer than about 3000 K (see his Fig. 11), so that Zr enhancements no doubt have to be present as well. The molecular spectra of cool S stars reflect as well both s-process enhancements and C/O effects. In that respect, it must be noted that the five Tc-rich S stars with the greatest ZrO indices ($I_{\rm ZrO} > 0.27$) are those having the most intense technetium lines (based on a visual inspection of the high resolution spectra of Paper I). The strength of the Tc line in these stars must be related to a large Tc (and hence s-process) abundance rather than to a temperature effect, since the temperatures of these 5 stars with strong Tc lines span the whole range observed for Tc-rich S stars (as derived from the $V-K$ colour index and the calibration of Ridgway et al. 1980). The large scatter in ZrO indices observed on the lower branch for a given value of the TiO index probably reflects the intrinsic scatter in s-process abundances among S stars.

5.3. Na D index and SC stars

An index based on the strength of the sodium D line is an useful complement (Ake 1979) to the TiO and ZrO indices described in Sect. 5.2. In carbon stars, the Na D lines are widely used as a temperature indicator; however, in S stars, the Na D index is sensitive to both temperature and abundances (Keenan & Boeshaar 1980), because of the opacity of overlying bands of ZrO, TiO, and CN.

Fig. 6 illustrates the trend of the Na D index with $B-V$ colour. For relatively low values (say, $I_{\rm NaD} < 0.6$), the Na D index is known to be a good temperature indicator (Keenan & Boeshaar 1980; Ake 1979). It is therefore not surprising that Tc-rich S stars, which are cooler than Tc-poor S stars, have on average larger Na D indices.

For larger values of the Na D index (say, $I_{\rm NaD} > 0.7$), the C/O ratio comes into play. At the top of the oblique sequence in Fig. 6 can be found the three SC stars of the Henize sample for which a low-resolution spectrum is available (Hen 120 = BH Cru = SC 4.5/8-e or SC 6/8-e or SC 7/8-e; Hen 135 = UY Cen = S 6/8- and Hen 157 = VY Aps; Catchpole & Feast 1971; Keenan & Boeshaar 1980); they are represented by an open star symbol in Fig. 6. The Henize stars populating the oblique sequence (from $I_{\rm NaD} > 0.7$) are closely related to SC stars, since they fulfill the spectral criteria defined by Catchpole & Feast

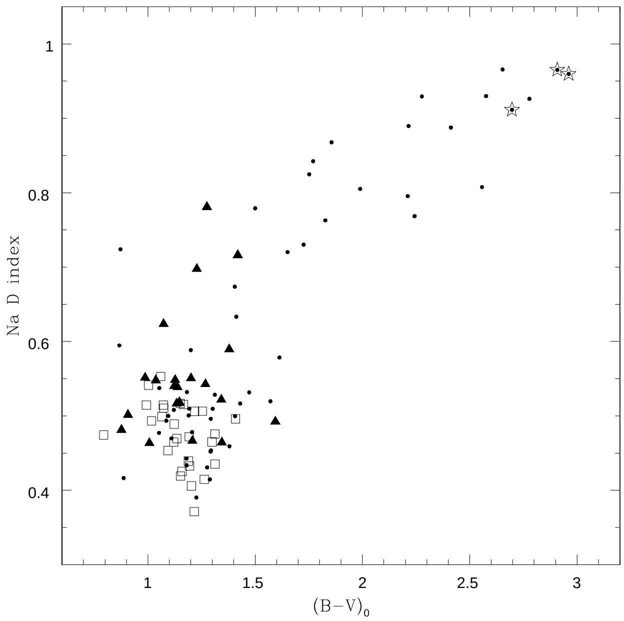

Fig. 6. Na D line index (as derived from low-resolution spectra with $S/N \geq 60$) versus the dereddened $B-V$ colour index. Symbols are as follows: open squares for Tc-poor S stars, filled triangles for Tc-rich S stars, dots for stars with unknown Tc. The three previously known SC stars (Hen 120 = BH Cru, Hen 135 = UY Cen, Hen 157 = VY Aps) are denoted by star symbols. Note that no technetium information is available from the current work for pure S and SC stars because of the very weak flux emitted by these stars below 4500Å, where the technetium resonance lines are located. Abia & Wallerstein (1998) however suggest that SC stars are Tc-rich, based on a quantitative analysis of the λ 5924.7 Å Tc I line

(1971): (i) extremely strong Na D lines, (ii) drop in the continuum intensity shortward of 4500Å, and (iii) bands of ZrO and CN simultaneously present (though quite weak), as well as general resemblance of the spectrum (i.e. regarding 'the absolute and relative strength of metal lines') with that of UY Cen = Hen 135.

Indeed, criterion (i) is automatically satisfied, since stars in the oblique sequence have large Na D indices ($I_{\rm NaD} > 0.7$), hence strong Na D lines. Criterion (ii) implies that SC stars have very red $B-V$ colour indices, since the effective wavelengths of the B and V filters are $\lambda_0(B) = 4227$Å and $\lambda_0(V) = 5488$Å (Rufener & Nicolet 1988). Therefore any flux deficiency occurring shortward of 4500Å results in a large $B-V$ colour index, as observed. Criterion (iii) is also fulfilled since the stars in the oblique sequence in Fig. 6 are those populating the upper sequence in Fig. 5, i.e., have weak TiO bands and weak to moderate ZrO bands.

The LaO bands provide an interesting additional piece of information indicating that the stars populating the oblique sequence in Fig. 6 cannot, though, be considered as genuine SC stars – except for the three previously-known

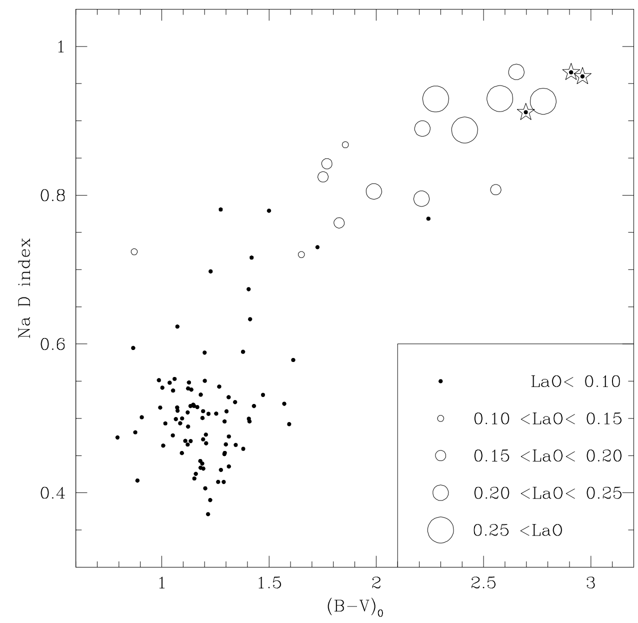

Fig. 7. Same as Fig. 6, but with symbols coding the strength of the LaO bands, as defined in Paper II. The three previously known SC stars (Hen 120 = BH Cru, Hen 135 = UY Cen, Hen 157 = VY Aps) are denoted by star symbols

SC stars (marked with a star symbol) – despite the resemblances mentioned above; rather, they are pure S stars.

The LaO bands are strong in stars with either a low effective temperature ($T_{\rm eff} \lesssim 2500$ K) or a C/O ratio close to unity within a few percents (Piccirillo 1977; Piccirillo 1980). As seen on Fig. 7, the LaO band strength is very weak in the bulk of S stars with $(B-V)_0 < 1.5$, increases with $(B-V)_0$ above $(B-V)_0 = 1.5$, but is markedly weak again for the three genuine SC stars at the upper right end of the oblique sequence in Fig.7. The absence of strong LaO bands in SC stars comes from the lack of free oxygen supply when C/O approaches unity. Therefore it is concluded that Hen 120, 135 and 157 are the *only* genuine SC stars among the 158 Henize stars for which low-resolution spectra are available.

As far as stars populating the oblique sequence are concerned, all the Westerlund-Olander stars of the Henize sample have strong LaO indices (as expected since this survey used the LaO bands to detect S stars) and fall on the oblique sequence [they all have $(B-V)_0 > 2.2$ and $I_{NaD} > 0.8$]. All these stars have been classified as S/5 or S/6 and are mostly pure-S stars (Lloyd Evans & Catchpole 1989). Hence the intermediate stars located on the oblique sequence of Fig.7 are believed to be nearly-pure or pure or cool S stars, and as such are intermediate between the bulk of S stars and SC stars.

6. Multivariate classification

6.1. The problem

The problem is to determine, among the 205 Henize S stars, which ones are the intrinsic (true TPAGB) stars, and which ones are the extrinsic (binary) stars. Since extrinsic and intrinsic S stars supposedly form two distinct classes of stars, with completely different evolutionary histories, it may be expected that they differ in many of their physical properties. The previous sections and Paper I have indeed shown that several observational parameters are potentially able to distinguish (with various efficiencies) intrinsic S stars from extrinsic S stars; the strengths and weaknesses of these various diagnostics are summarized in Table 1.

The problem in hand is typically one of multivariate classification: N objects (the Henize sample of 205 stars) need to be classified according to m parameters (as listed in Table 1).

Among the plethora of multivariate data analysis techniques (see e.g. Murtagh & Heck 1987), cluster analysis seems the best suited to the present problem, since it actually builds up the various groups when no group assignment is available a priori (it is an *unsupervised* classification method). Partitioning methods have been preferred over hierarchical methods: indeed, the former provide the best clustering for a given number of clusters, whereas the latter build up the clusters step after step, starting with every object in a different cluster, and then clustering together the most similar objects until one single cluster containing all the objects is obtained[2]; such hierarchical techniques can never repair what was done in the previous steps, and provide no guarantee that the best possible clustering for a given number of clusters has been obtained.

An additional complication comes from the incompleteness of our data set: not all the observational parameters are available for all the 205 stars. Such missing values prevent the blind application of any multivariate classification method. In fact, the widely recommended solution is to ignore completely objects that have *any* missing values. This option is not affordable here: it would reduce the sample size dramatically (e.g. only 70 stars out of 205 have the vital technetium data available), and would throw away an intolerably large amount of valuable information. Another alternative is to employ *imputation*, that is the insertion of an estimate for each missing value, thereby completing the data set. In the present case, such imputations could lead to seriously underestimating the variances, and blur or even erase the separation between intrinsic and extrinsic stars. A totally different method to handle stars with missing values has thus been designed, as described in Sect. 6.2.

[2] this is "agglomerative" clustering; for the opposite clustering direction, algorithms are named "divisive".

Table 1. Observational data, their discriminating power and their limitations

observational data	extrinsic stars	intrinsic stars	limitations	Ref.
• technetium	no	yes	only available for 70 stars (the bluest and/or brightest)	Paper I
• radial velocity	periodic variations	jitter	poor orbital coverage or unfavorably oriented orbits (pole-on) hinder the detection of extrinsic S star variability, while radial velocity jitter may mimic orbital motion for intrinsic S stars	Sect. 2.2
• shape of the CORAVEL cc-dip	deep and narrow	shallow and wide	fuzzy extrinsic/intrinsic boundary	Sect. 2.1
• UBV photometry	blue, non-variable	red, variable	blue Miras confuse the classification; lack of measurements for faint stars	Sect. 3.1
• IRAS	K-[12]<0.9 K-[25]<0.9	often K-[12]>0.9 often K-[25]>0.9	relatively few good-quality fluxes, especially for extrinsic stars	Sect. 4
• low-resolution spectroscopy	relatively weak TiO, ZrO and Na D	strong TiO or ZrO, strong Na D	fuzzy extrinsic/intrinsic boundaries; only available for 158 stars	Sect. 5

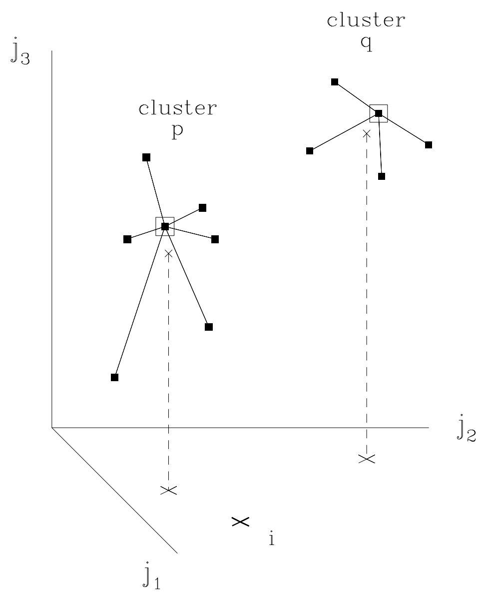

Fig. 8. Schematic illustration of clustering (in a three-dimensional Euclidian parameter space j_1,j_2,j_3) for a uncomplete star i with parameter j_3 missing. The open squares indicate the best representative star of each cluster, the small crosses their center of gravity, and the large crosses the projection of their center of gravity on the subspace (j_1, j_2) of star i

6.2. The clustering algorithm

After a careful examination of the various available techniques, the clustering program CLARA described in Kaufman & Rousseeuw (1990) has been chosen and further adapted in order to classify *all* the stars, the *complete* stars (i.e., those stars having all the m parameters available on which clustering is performed) as well as the *uncomplete* ones (stars with some missing parameters).

The classification proceeds along the following steps:

1. The data are first normalized in order to avoid dependence on the measurement units: if x_{ij} is the j^{th} parameter of star i, $\overline{x}_j$ the mean value of the j^{th} parameter for all the stars, and σ_j its standard deviation, then the normalized value is computed as: $x'_{ij} = (x_{ij} - \overline{x}_j)/\sigma_j$
2. In order to quantify the degree of dissimilarity between stars i_1 and i_2, the Euclidian distance $d(i_1, i_2)$ is computed:

$$d(i_1, i_2) = \left[\sum_{j=1}^{m}(x'_{i_1j} - x'_{i_2j})^2\right]^{1/2}$$

3. The number k of desired clusters is fixed in advance.
4. A seed sample of stars is drawn from the entire star set. In the original program CLARA, many random seed samples were successively chosen and the best resulting clustering was retained. In the present case, due to the many incomplete stars, a better strategy is to choose only one seed sample, once for all, as the sample of complete stars (Rousseeuw, priv. comm.). The CLARA program has thus been modified to this end.

5. The method then selects k stars, called *representative stars*, within the seed sample of complete stars. The k clusters are then constructed by assigning each complete star of the data set to the nearest representative star.
   Of course, not every selection of k representative stars gives rise to a subsequent "good" clustering. The *optimal representative stars* will be those for which the average distance of the representative star to all the other (complete) objects of the same cluster is minimum. For a full description of the algorithm finding the optimal representative stars, we refer to Chapter 2 of Kaufman & Rousseeuw (1990).
6. The clusters are then completed by assigning each remaining uncomplete star to the nearest cluster: the distance between any uncomplete star and each cluster center of gravity (projected on the subspace where the uncomplete star is located, see Fig. 8) is computed; the uncomplete star is agglomerated to the cluster that minimizes this distance. In Fig. 8, this means that star i will be assigned to cluster p.

This algorithm is especially suitable here because it provides a representative star for each cluster, a very desirable feature for characterization purposes. The drawback of such an approach is that the representative stars of each cluster are chosen among complete stars only, hence they are not necessarily optimal representative of the uncomplete stars as well. The risk is thus to agglomerate some 'exotic' uncomplete star to some existing cluster (from which it is the closest on the basis of its available parameters), although this exotic star should in fact have been the seed of a new cluster. However, we feel this risk is rather unimportant given the purpose of the classification (distinguishing intrinsic from extrinsic S stars), because the available parameters of uncomplete stars often match correctly the corresponding parameters of complete stars. It might happen that some stars have outstanding photometric variations or very red colours, but these extreme stars will be automatically classified in the intrinsic groups, which is a correct assignment since such evolved stars are very unlikely to be extrinsic S stars.

Misclassifications can never be excluded by such clustering techniques. However, their major advantage over a 'handmade' classification lies in that they guarantee that the classification criteria will remain homogeneous for the 205 stars: all the available parameters will be taken into consideration in the same way from the first star to the very last.

6.3. Classification parameters

The number of parameters m used in the clustering is critical. It should not be too small, in order to limit the number of stars with none of the parameters available. Neither should it be too large, in order to maximize the number of complete stars and therefore to achieve a better definition of the clusters. Moreover, the classification parameters must have a real discriminating power, otherwise they will blur the work done by the other more useful parameters.

After trials and errors, 10 parameters have been retained as giving the best possible clustering, i.e., the smallest number of obviously misclassified stars. These parameters, whose discriminating power was discussed in the previous sections (see also Table 1), are: technetium, the width (Sb) and depth (PR) of the CORAVEL cc-dip, the radial velocity standard deviation $\sigma(V_r)$, the $(U-B)_0$, $(B-V)_0$, and K-[12] colour indices, and the photometric standard deviation $\sigma_{phot} = (\sigma(B)^2 + \sigma(V)^2)^{1/2}$. An "abundance index" $I = I_{ZrO} + I_{TiO} + I_{NaD}$ has also been included: as shown in Figs. 5 and 6, it remains small for Tc-poor stars, increases somewhat for Tc-rich stars because of slightly stronger TiO bands and/or ZrO bands, and reaches its highest values for pure S and SC stars, because of their strong Na D lines. The $(V-K)_0$ index has also been added in the parameter list because Tc-poor S stars often have bluer $(V-K)_0$ colours than Tc-rich S stars.

This choice results in 196 stars out of 205 having at least one parameter available, among which 33 stars have all of them available ("complete" stars). The 2 misclassified S stars Hen 22 and Hen 154 (Sect. 5.1) have been excluded from the cluster analysis. The 7 remaining stars with no classification parameters available are:

– Hen 26, Hen 60, Hen 102 (=TT10) and Hen 116: no data whatsoever have been obtained for these stars in the present work. Hen 116 ($\alpha_{1900} = 11^h43^m.0; \delta_{1900} = -64°46'$ according to the unpublished list of Henize (1965)) is not considered as an S star by Stephenson (1984; see his Table 2). The other three stars may well be variable stars; however, without any piece of information to classify them, they have been excluded from the cluster analysis.
– Hen 33 and 176 are clearly located among intrinsic stars in the ([12]-[25],[25]-[60]) IRAS colour-colour diagram (Jorissen et al. 1993). Henize classified Hen 33 as an S5,8e star, which is more typical of intrinsic stars also. In the same vein, Hen 192 has a [12]-[25] index typical of intrinsic stars. These three stars are therefore *a posteriori* included in the intrinsic group.

6.4. Clustering analysis: results

The number of clusters is also critical. Therefore clustering analyses with two and six clusters are presented and compared in Sects. 6.4.1 and 6.4.2, respectively.

6.4.1. Two clusters

Since the S family is suspected to comprise two kinds of stars, clustering has first been attempted with two clusters. Their center of gravity is listed in Table 2, and individual assignments are provided in Paper II. The correctness of the individual star assignments to one or the other cluster – and the possible ways to check it – will be discussed in more details in Sect. 6.5. At this point, it will just be mentioned that the clustering analysis with two clusters leads to only one clearly misclassified star (Hen 152) and one puzzling case (Hen 189). Hen 152 has many characteristics of an intrinsic star, although it was classified in the extrinsic group. The reason for that misclassification lies in the two extremely discrepant radial velocity measurements [$\sigma(V_r) = 9$ km s^{-1}], which brings the star near to the extrinsic group. In fact Hen 152 is most probably a pure S or SC star, because of its huge cc-dip width (Sb=16 km s^{-1}), very red colours [$(B-V)_0 = 2.6$] and large photometric variability ($\sigma_{phot} = 0.6$ mag).

Hen 189 is a puzzling case that has been classified in the intrinsic group by the algorithm. Indeed it is clearly different from "normal" extrinsic stars, because of its larger photometric variability. Its blue colours may tag it as either a symbiotic star or a blue Mira; however, its deep and narrow cc-dip is not typical of Miras. Given the lack of further information, it was kept in the intrinsic group.

6.4.2. Six clusters

Is it possible to further split the intrinsic and extrinsic classes into more subgroups? A classification with six clusters leads to relatively well-defined groups indeed. These groups and their center of gravity are listed in Table 2. However this subdivision does *not* mean that these six groups correspond to six types of physically-different stars. For example, the clustering algorithm produces two groups (#1 and #2) of extrinsic stars differing mainly in their radial-velocity standard deviations. Both groups are believed to contain binary stars, but group #2 contains more orbits closer to edge-on and/or with shorter periods and/or with a better sampling of the radial-velocity measurements, resulting in larger radial-velocity standard deviations.

The clusters are not as widely separated as in the two-clusters case. Hence more stars (4) are erroneously classified: Hen 49 and 152 are clearly misclassified as extrinsic stars, probably because of their large radial-velocity standard deviation or their unusual photometric behaviour. In fact they rather resemble pure S or SC stars. Hen 15 and 117 have been classified in the symbiotic group, though they are rather intrinsic stars; the reason here is probably the lack of data on these faint stars. In Table 6 of Paper II, these 4 stars have been re-assigned to the 'second-best-choice' cluster determined by the algorithm, which is in these four cases an intrinsic cluster.

All stars with less than 5 parameters available were examined individually; their classification seems to be correct.

The six-clusters classification may be compared to the two-clusters classification, by merging groups #1, 2, and 3 in the same extrinsic (Tc-poor) category, and groups #4, 5 and 6 in the same intrinsic (Tc-rich) category. The same partitioning of the Henize sample is found as in the two-clusters case, except for 3 stars: Hen 46, 67 and 189 were previously classified in the intrinsic group and are now in the extrinsic group. These three stars are typical borderline cases (Hen 189 has been discussed above) and it is indeed very difficult to determine if they belong to the intrinsic group or to the extrinsic one with the available data. It is however encouraging that the clustering algorithm yields identical results for the 193 remaining stars, separating in distinct groups intrinsic and extrinsic stars.

The group properties may be summarized as follows:

1. Extrinsic stars:
   - group 1: Tc-poor stars: narrow and deep cc-dip, UBV magnitudes almost constant and colours close to that of normal giants, photospheric IRAS colours, small abundance index I.
   - group 2: same as group 1, except for smaller radial-velocity standard deviations.
   - group 3: symbiotic stars, large-amplitude binaries and with extremely blue and variable photometric indices.
2. Intrinsic stars:
   - group 4: "the less evolved" Tc-rich stars: the cc-dip is wider and shallower than in the (non-symbiotic) extrinsic groups, but not as distorted as in the other intrinsic groups (a typical example is Hen 97 in Fig. 1); the stars exhibit a moderate photometric variability and radial-velocity jitter, and redder colours than the extrinsic stars.
   - group 5: Tc-rich stars, intermediate between groups 4 and 6, with many blue Miras.
   - group 6: Tc-rich stars with strongly distorted cc-dips, strongly variable UBV photometry and large radial-velocity jitter. They present the highest values of the abundance index I and large infrared excesses.

6.5. Testing the validity of the cluster assignments

Technetium provides a way to check the quality of the classification presented in Sect. 6.4. Technetium is at the origin of the division of the S star family into extrinsic and intrinsic stars. Hence, if that division is sound, Tc-poor and Tc-rich stars should not be mixed in any given cluster. This is indeed the case. Even though technetium is one of the classification parameters, this result was not guaranteed *a priori*, because the nine other parameters

Table 2. Cluster average properties. The cluster reference number is indicated in the first column, the number of stars in each cluster comes in the second column and the average value of the 10 classification parameters (see text) are listed next. The last column indicates the intrinsic or extrinsic nature of the considered cluster (based on its Tc content). In the 6-clusters classification, clusters have been ordered according to increasing *Sb* values.

	N	Tc	Sb	PR	$\sigma(V_r)$	$(U-B)_0$	$(B-V)_0$	$(V-K)_0$	σ_{phot}	I	K-[12]	
• 2 clusters												
1	63	no	4.72	0.38	3.23	3.14	1.20	5.07	0.06	0.94	0.65	ext
2	133	yes	7.96	0.27	1.98	2.89	1.65	7.07	0.42	1.42	1.19	int
• 6 clusters												
1	15	no	4.48	0.39	6.00	3.18	1.15	4.43	0.04	0.91	0.61	ext
2	49	no	4.77	0.38	2.20	3.18	1.22	4.78	0.06	0.95	0.67	ext
3	2	no	5.83	0.23	6.74	1.66	0.89	5.56	0.17	1.14	0.67	ext, symb
4	55	yes	6.66	0.33	1.41	3.24	1.64	5.78	0.19	1.23	0.91	int
5	12	yes	7.95	0.17	1.88	2.10	0.88	6.86	0.31	1.18	1.11	int
6	63	yes	10.00	0.22	2.82	2.77	1.84	7.42	0.71	1.64	1.50	int

could easily blur the discriminating action of technetium, if there were no genuine underlying dichotomy in the S family.

This check may be applied to the 37 incomplete stars (among 163) having nevertheless Tc data. This subsample of incomplete stars may be considered as a *test subsample*, because the clusters are defined independently of it (since they are defined from *complete* stars only, see Sect. 6.2). All these uncomplete stars are correctly classified, i.e., they are assigned to Tc-rich or Tc-poor clusters in agreement with their Tc content, despite the possible blurring action of the other parameters.

This result ensures that there is no major flaw in the clustering algorithm used in the present paper.

The classification finally retained is that with six clusters, where clusters 1, 2 and 3 are merged in the extrinsic class, and clusters 4, 5 and 6 constitute the intrinsic class. The three intrinsic stars Hen 33, 176 and 192 (with none of the classification parameters available) are incorporated in the intrinsic class (see Sect. 6.3). Hence the Henize sample of 205 stars comprises 66 extrinsic stars, 133 intrinsic stars, 4 unclassified stars and 2 non-S stars.

7. Radial-velocity variations in the Henize sample

The histograms of the radial-velocity standard deviation for intrinsic and extrinsic S stars are presented in Fig. 10. The intrinsic and extrinsic groups are separated according to the clustering algorithm described in Sect. 6.4.2.

The distribution of the standard deviation of the radial-velocity measurements for intrinsic S stars is strongly peaked at $\sigma(V_r) \sim 1.5$ km s^{-1} and is rapidly falling off at larger $\sigma(V_r)$. It probably reflects the jitter associated with the unstable atmosphere of pulsating AGB stars. The lack of intrinsic S stars with $\sigma(V_r) < 0.5$ km s^{-1} is also clearly visible.

On the contrary, the $\sigma(V_r)$ distribution for extrinsic S stars is much flatter, and this feature is, as expected, a clear signature of the large frequency of binaries among extrinsic S stars. The stars with $\sigma(V_r) < 0.5$ km s^{-1} are probably long-period and/or nearly pole-on binaries.

8. Galactic distribution

8.1. Extrapolation to the complete sphere

The Henize sample is limited on the sky by the simple criterion $\delta < -25°$. Translating this condition into galactic coordinates reveals that the latitudes surveyed go from $b = +37°$ down to the south galactic pole – a very desirable feature for estimating the galactic scale height of S stars (Fig. 11).

The unequal galactic longitude coverage $\Delta l(b)$ at different galactic latitudes b in the Henize sample has been corrected by assigning a weight $P_\star$ to each star, defined as the inverse fraction of the circumference covered by the Henize sample at the star's latitude, for both hemispheres: $P_\star(|b|) = 2 \times 360°/[\Delta l(|b_\star|) + \Delta l(-|b_\star|)]$ (the distribution of S stars is assumed to be symmetric with respect to the galactic equator and independent of l). In other words, $P_\star(|b|)$ is the *effective number* of S stars at latitudes $|b|$ and $-|b|$, and the sum of the weights of all the stars of the Henize sample gives the total number of S stars that would have been detected if the whole galactic sphere had been surveyed (with a limiting magnitude $R = 10.5$), i.e., 626.

8.2. Distances

Distances were computed from the bolometric distance modulus, adopting $M_{\rm bol} = -3.1$ and -4.4 for extrinsic and intrinsic S stars, respectively (Van Eck et al. 1998). The apparent bolometric magnitudes have been computed

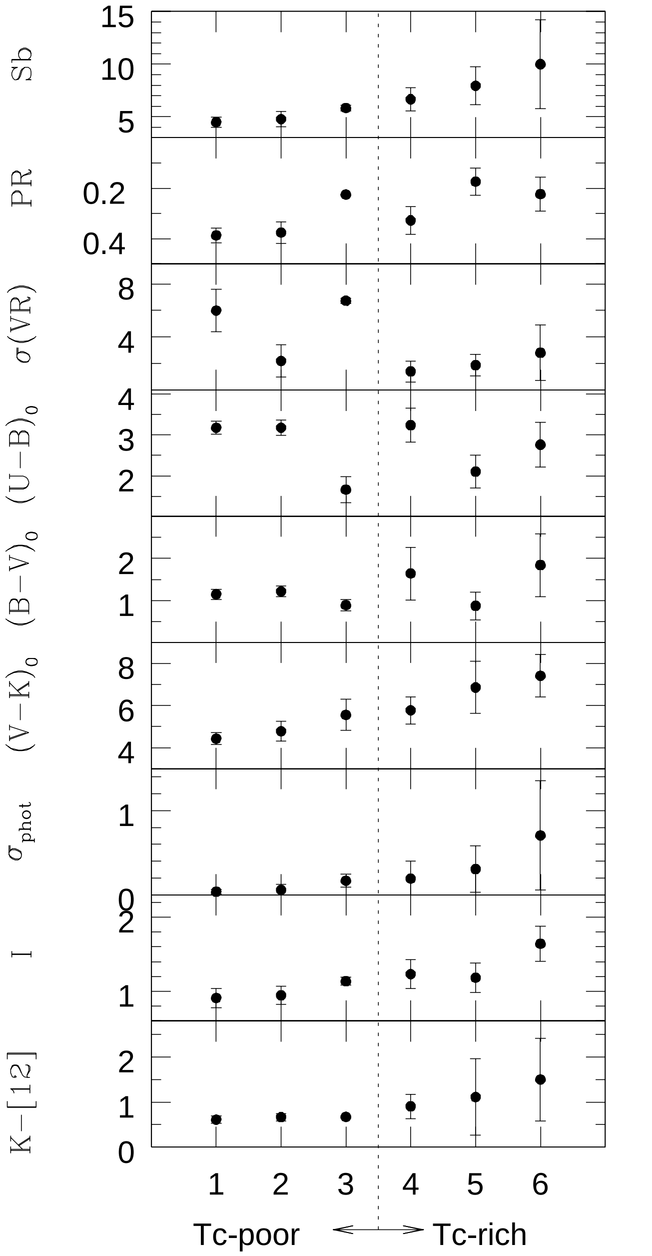

Fig. 9. Average values and standard deviation (represented as error bars) of the 9 parameters used to derive the 6 clusters. The tenth parameter used in the clustering, technetium, is indicated at the bottom. Notice the smooth evolution of the parameters from one cluster to the next (with the exception of group #3 which consists of the two symbiotic stars)

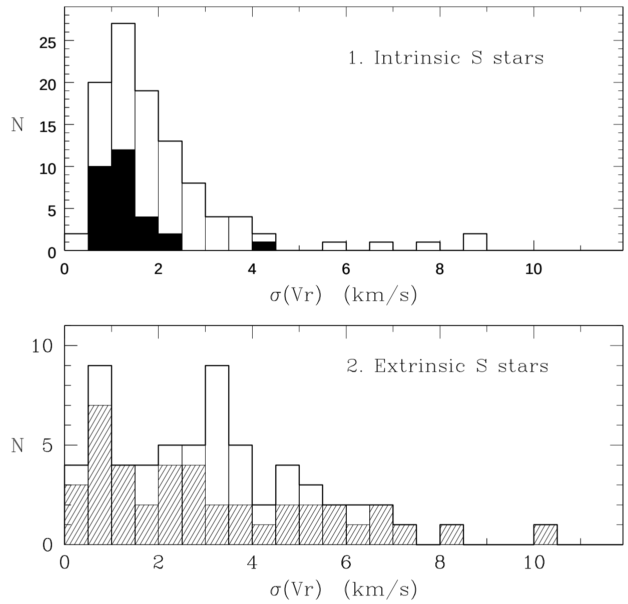

Fig. 10. Histogram of the standard deviation $\sigma(V_r)$ of the radial velocity measurements for the S stars of the Henize sample. The intrinsic S stars (top) and extrinsic S stars (bottom) are separated according to the clustering algorithm presented in Sect. 6.4.2. Tc-rich and Tc-poor S stars are represented in black and hatched bins, respectively. The upper and lower histograms have different envelopes: the long tail of extrinsic S stars with large radial-velocity standard deviations (lower panel) reflects the binary nature of these stars

for 126 Henize S stars by integrating the spectral energy distribution derived from the U, B, V, J, H, K and L bands (Paper II).

The sampling distance of the Henize sample must be estimated from its limiting magnitude $R = 10.5$. This limiting magnitude must first be dereddened by using the average $B-V$ colour excess (see Sect. 3.3 of Paper II) for extrinsic ($E_{B-V} = 0.15$ mag) and intrinsic stars ($E_{B-V} = 0.24$ mag). The extinction law of Cardelli et al. (1989) then yields $A_R = 0.34$ and 0.57 mag for extrinsic and intrinsic stars, respectively. The bolometric correction $BC_R = m_{\rm bol} - R$ to be applied to the R band writes $BC_R = -0.4(V-K)_0 + 1.33$, as estimated from a least square fit for the sample of S stars with $m_{\rm bol}$ and $(V-K)_0$ available in Table 1 of Van Eck et al. (1998) and R collected from the literature. Given the average $(V-K)_0$ colour indices of extrinsic and intrinsic S stars [$(V-K)_0 = 4.7$ for clusters # 1, 2 and 3 (extrinsic stars); $(V-K)_0 = 6.5$ for clusters # 4, 5 and 6 (intrinsic stars); see Sect. 6.4.2] and the limiting R magnitudes of Henize's extrinsic and intrinsic stars, the limiting apparent bolometric magnitudes amount to $m_{\rm bol,lim} = 9.6$ for extrinsic S stars and $m_{\rm bol,lim} = 8.6$ for intrinsic S stars. Adopting reasonable absolute bolometric magnitudes of -3.1 and -4.4 for extrinsic and intrinsic S stars, respectively (Van Eck et al. 1998), we find that the maximum distances to which S stars have been observed in the Henize sample are 3.5 kpc for extrinsic S stars and 4.1 kpc for intrinsic S stars.

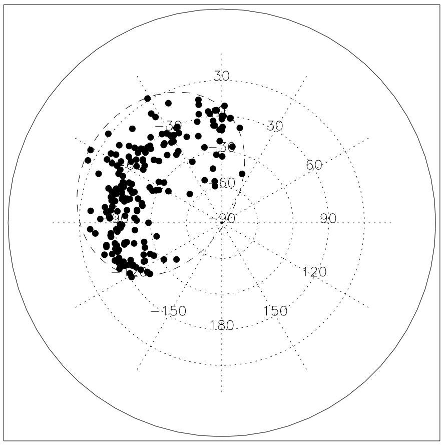

Fig. 11. On this azimuthal projection of the Henize sample of S stars, the south galactic pole is located at the center. Concentric circles correspond to galactic latitudes $-60°$, $-30°$, $0°$ and $30°$. The long-dashed line represents the limit $\delta = -25°$, and shows that the south galactic pole has been fully surveyed

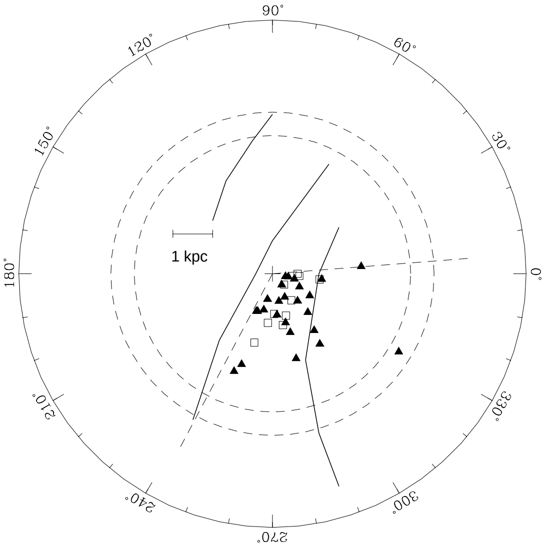

Fig. 12. Projection of the Henize S stars on the galactic plane (the galactic center falls outside the frame towards the right; the central cross represents the position of the Sun). Only those stars with $|z| < 100$ pc have been retained. Black triangles stand for intrinsic stars, whereas open squares represent extrinsic stars, as derived from the 6-cluster classification (Sect. 6.4.2). The three solid lines correspond to the galactic arms Perseus, Orion and Sagittarius from Vogt & Moffat (1975). The dashed straight lines correspond to the boundaries of the Henize sample in the galactic plane ($\delta < -25°$) and the dashed circles to the sampling distances of 3.5 kpc (extrinsic S stars) and 4.1 kpc (intrinsic S stars)

8.3. Distribution on the galactic plane

The projection of Henize S stars onto the galactic plane is plotted in Fig. 12, along with the estimated sampling distance (Sect. 8.2). Although these sampling distances might appear somewhat overestimated when compared to the distance of the farthest detected star, it must be noted that Fig. 12 displays only those stars for which the apparent bolometric magnitude could be derived from direct integration of the *UBVJHKL* fluxes (Sect. 8.2). Hence, 79 out of 205 stars have not been considered on Fig. 12, and those stars with missing *UBV* or *JHKL* data are precisely the faintest, i.e., farthest, objects. Therefore, the maximum sampling distance displayed on Fig. 12 will nevertheless be considered as correct and will be used in the following.

In the first study ever of the galactic distribution of S stars, Keenan (1954) found that S stars (excluding long-period variables) fall along spiral arms (as mapped by Morgan et al. 1953). Before 1965, there was a general consensus that the non-Mira S stars were spiral-arm objects or were found in OB associations, hence that they were younger than the majority of M giants (Nassau 1958; Takayanagi 1960). However, as noted by Yorka & Wing (1979), no systematic surveys for S stars at high galactic latitudes had yet been published, causing a strong bias in the available data.

The situation in that respect improved dramatically thanks to the Henize survey (Henize 1960), Wray's thesis (Wray 1966) and various red and near-infrared objective-prism surveys conducted at the Warner and Swasey Observatory (see Stephenson 1984). In their study of the galactic distribution of S stars using this material, Yorka & Wing (1979) found no concentration of S stars in the galactic plane as strong as that of extreme Population I objects, nor any association with the galactic arms or interstellar clouds.

The present work, based solely on the Henize sample, but distinguishing extrinsic S stars from intrinsic S stars, confirms their finding, since Fig. 12 shows no clear evidence for a concentration of either kind of S stars along the galactic arms.

8.4. Galactic scale heights

The density distribution of extrinsic and intrinsic S stars as a function of the height z above the galactic plane is displayed in Fig. 13. It has been computed from the observed star counts in the bin $(z, z + dz)$ multiplied by the weights $P_\star(|b|)$ (Sect. 8.1), divided by the volume $\pi \times (d_S^2 - z^2) \times dz$ sampled for the given bin $(z, z + dz)$, where d_S is the sampling distance estimated in Sect. 8.2 and $z = d_S \sin b$.

The upper two panels of Fig. 13 present the density distribution for the stars whose distances could be derived from the bolometric apparent magnitudes computed from the *UBVJHKL* fluxes (as explained in Sect. 8.2). The density distribution has been normalized to its value in

Table 3. Exponential scale heights z_0 for extrinsic and intrinsic S stars derived by various methods (see text)

	m_{bol}	N(ext)	N(int)	$M_{\rm bol}$(ext)	$M_{\rm bol}$(int)	z_0(ext) (pc)	z_0(int) (pc)
a.	$\int$ UBVJHKL	51	75	-3.1 ± 1.0	-4.4 ± 1.0	$580\,^{-210}_{+320}$	$220\,^{-60}_{+120}$ ($z \leq 1000$ pc)
b.	$\int$ UBVJHKL V_0 <10	34	38	-3.1	-4.4	560	180
c.	$\int$ UBVJHKL V_0 <8.5	11	10	-3.1	-4.4	810	260
d.	$V_0 + BC_V$	65	105	-3.1	-4.4	520	170
Adopted						600 ± 100	200 ± 100

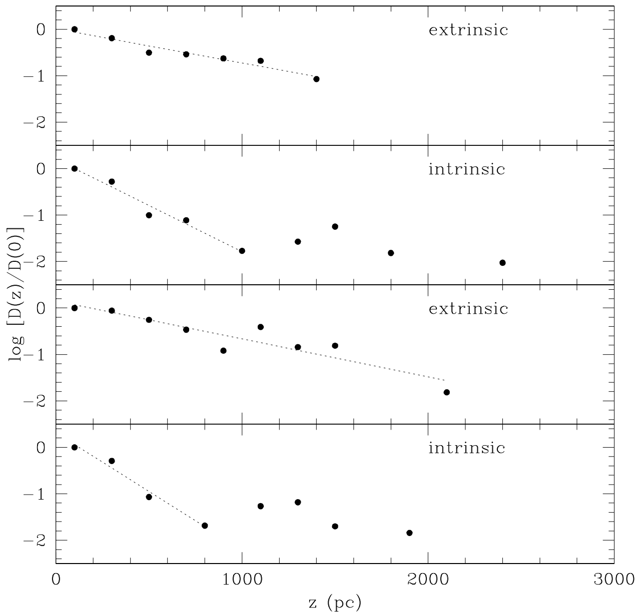

Fig. 13. Logarithm of the density distribution perpendicular to the galactic plane for intrinsic and extrinsic S stars, normalized to the density in the plane. In the upper two panels, the distances were derived from the apparent bolometric magnitudes computed by integrating the $UBVJHKL$ fluxes. In the lower two panels, the apparent bolometric magnitudes were derived from V and a bolometric correction derived separately for each of the clusters of Table 2 (see text)

the galactic plane so as to make it roughly independent from the estimated sampling distance (as long as $z \ll d_S$). However, the scale heights will nevertheless still depend upon the adopted absolute bolometric magnitude.

Adopting $M_{\rm bol} = -4.4 \pm 1.0$ and $M_{\rm bol} = -3.1 \pm 1.0$ for intrinsic and extrinsic stars, respectively, exponential scale heigths of $220\,^{-60}_{+120}$ and $580\,^{-210}_{+320}$ pc are obtained (case a of Table 3). Note that in the case of intrinsic S stars, points above $\sim$ 1000 pc do not follow the exponential distribution defined from the star counts closer from the plane. They cannot be explained by invoking a contamination of the intrinsic sample by extrinsic stars, because the 6 stars responsible for these four outlying points above $\sim$ 1000 pc are probably all intrinsic stars (2 are Tc-rich, none is Tc-poor). In fact, these outlying points probably result from the larger uncertainties altering the distances of these faint stars.

The above scale heights were derived from the subsample of 126 stars (out of 205 Henize S stars) for which the apparent bolometric magnitude could be reliably determined from the integration of the $UBVJHKL$ fluxes. In order to evaluate whether or not the scale heights derived from this particular subsample are somehow biased, scale heights derived from other subsamples are now computed.

First, the scale heights were determined for subsamples of different V_0 limiting magnitudes extracted from the complete Henize sample. For example, in the Henize subsample limited to stars brighter than $V_0 = 10$ (72 stars), the bolometric magnitude is available for 85% of the stars; the derived scale heights are listed in case b of Table 3, and in case c if the limiting magnitude is $V_0 = 8.5$. The scale heights derived from these smaller albeit internally more complete samples still lead to a significant scale height difference between extrinsic and intrinsic S stars.

Second, the considered sample has been enlarged by deriving the apparent bolometric magnitudes from the V magnitude and the corresponding bolometric correction. That correction has been calibrated separately for each of the 6 clusters of S stars provided by the clustering algorithm (Table 2), from the stars that have a reliable apparent bolometric magnitude available from the integration of the $UBVJHKL$ fluxes (i.e., belonging to sample a). Although that method allows to increase the sample to 170 stars (instead of 126 for sample a), the drawback is that the derived apparent bolometric magnitudes – and hence, the distances – are far less accurate, since the V filter catches only a small fraction of the total flux emitted by these red stars.

The corresponding density distributions are displayed in the lower two panels of Fig. 13, and the derived scale heights are listed in case *d* of Table 3. The difference between these scale heights and the previous ones is not surprising, given the much lower precision of the adopted bolometric magnitudes. However they confirm on a larger subsample that *the intrinsic S stars are much more concentrated towards the galactic plane than are the extrinsic S stars.*

Could this difference in scale height be spurious, and caused by our particular choice of the absolute bolometric magnitudes? Van Eck et al. (1998) have stressed that the average bolometric magnitudes of intrinsic and extrinsic S stars, as derived from HIPPARCOS data, are subject to various biases which render these absolute magnitudes still somewhat uncertain. In order to force extrinsic and intrinsic S stars to have the same scale height, one has to impose a difference of nearly 4 magnitudes between their average absolute magnitudes (e.g., $M_{\rm bol,ext} = -2$ and $M_{\rm bol,int} = -6$, yielding an identical scale height of ~ 350 pc). Despite the remaining uncertainties on $M_{\rm bol}$ mentioned above, such a large difference in the bolometric magnitudes of extrinsic and intrinsic S stars is definitely incompatible with the available HIPPARCOS data (if anything, the existing biases would rather tend to decrease the observed gap between the average $M_{\rm bol}$ of extrinsic and intrinsic S stars; see Fig. B in Appendix B of Van Eck et al. 1998).

Hence the difference in scale heights between extrinsic and intrinsic S stars is undoubtedly real, revealing that intrinsic and extrinsic S stars clearly belong to two different populations. Given the various estimates presented in Table 3 and their uncertainties, the adopted exponential scale heights are 600 ± 100 pc for extrinsic S stars and 200 ± 100 pc for intrinsic S stars. In fact, the scale height for intrinsic S stars happens to be comparable to that of planetary nebulae. Zijlstra & Pottasch (1991) derive an exponential scale height of 250 ± 50 pc. This good agreement is not unexpected since intrinsic S stars will shortly (i.e., within the duration of the TPAGB, which is short compared to the total stellar lifetime) eject their envelope and become planetary nebulae. It is also similar to the scale heights ($\sim 230 - 250$ pc) estimated for O-rich SRa, SRb and long-period ($P > 300$ d) Mira stars (Kerschbaum & Hron 1992, Jura & Kleinmann 1992a,b). The exponential scale height of intrinsic S stars is in any case typical of disk stars, but the uncertainty on our determination precludes any detailed identification of the progenitors of intrinsic S stars with either massive or low-mass main sequence stars. The exponential scale height of intrinsic S stars quoted in Table 3 (200 ± 100 pc) in fact encompasses values typical of both the young and old disks (see Fig. 5 of Gilmore & Reid 1983).

As far as extrinsic S stars are concerned, their exponential scale height of 600 ± 100 pc is smaller than the values usually quoted for the extended/thick disk (about 1400 pc; see the discussion of Reid & Majewski 1993). Nevertheless, it is similar to the scale height of short-period ($P < 300$ d) Miras (Jura 1994; Kerschbaum & Hron 1992), although that group may be a mixture of thin-disk and extended-disk stars having different metallicities and scale heigths (Norris & Green 1989; Hron 1993). According to Norris & Green (1989, their Table 8), an exponential scale height of 600 ± 100 pc is typical of giants with metallicities in the range [Fe/H]$= -0.5$ to -0.4.

Catchpole & Feast (1985) also found that different subclasses of S stars are characterized by different scale heights (z=195, 600 and 680 pc for 27 SC stars, 29 Se stars and 124 S stars respectively), although these results are difficult to compare with ours since they correspond to a different partition of the S star family.

9. The relative frequency of extrinsic/intrinsic S stars

9.1. Magnitude-limited sample

In the magnitude-limited Henize sample of 205 S stars, the separation of extrinsic and intrinsic S stars on the basis of the clustering algorithm described in Sect. 6 leads to 66 extrinsic S stars, 133 intrinsic S stars, 2 misclassified S stars, and 4 stars with no information at all (Hen 26, 60, 102, 116).

When correction is made for the unequal galactic longitude coverage at different galactic latitudes (see Sect. 8.1), the percentages of extrinsic and intrinsic S stars are 66 ± 5% and 34 ± 5%, respectively, given the 4 unclassified stars and the estimated uncertainties on the clustering technique.

9.2. Volume-limited sample

9.2.1. Estimate 1: in the entire Henize sample

The relative frequency of extrinsic and intrinsic S stars in a volume-limited sample is subject to far more uncertainties, because it depends directly upon the estimated sampling distance. As noted above, the Henize sample comprises extrinsic S stars up to ~ 3.5 kpc and intrinsic S stars up to ~ 4.1 kpc. The respective surface densities of intrinsic/extrinsic S stars projected onto the plane then correspond to the total number of S stars of a given kind (extrapolated to all longitudes; Sect.8.1) divided by the area sampled in the plane (since the scale height is much smaller than the sampling distance). The relative surface densities are then 42 ± 1% for extrinsic S stars and 58 ± 1% for intrinsic S stars. Large uncertainties affect these frequencies; in fact, by pushing all the uncertainties to their worst limits, the percentage of extrinsic stars can lie anywhere between 20 and 90%!

9.2.2. Estimate 2: in the solar neighbourhood

The relative star density in the solar neighbourhood, as derived from the normalization used in Fig. 13, is $D(0)_{int}/D(0)_{ext} = 2.3$, which leads to 30% of extrinsic stars and 70% of intrinsic stars. The higher fraction of intrinsic S stars with respect to extrinsic S stars is compatible with their greater concentration in the galactic plane, as derived in Sect. 8.4. Note that, unlike the scale heights derived in Sect. 8.4, the ratio $D(0)_{int}/D(0)_{ext}$ is directly affected by possible errors on the sampling distances.

9.2.3. Estimate 3: in a 1.5 kpc sphere

A frequency estimate independent of the sampling distance – subject to large uncertainties – may be obtained by considering the respective numbers of extrinsic and intrinsic S stars in a sphere of radius 1.5 kpc. Such a sphere is small enough to ensure completeness for both the extrinsic and intrinsic samples, and large enough with respect to the exponential scale heights to include most stars of both classes.

When using the apparent bolometric magnitudes derived from the V magnitude (as in case d of Table 3), the frequency of intrinsic S stars is estimated to be 55%.

9.3. The Henize survey as compared to other surveys

Fig. 14 compares the V magnitude and galactic-latitude distributions of several samples of S stars, as listed in Stephenson (1984). The Henize survey, as listed in Stephenson (1984), is probably the only homogeneous magnitude-limited survey that extends from the galactic plane up to high galactic latitudes. Nevertheless, other surveys subsequently detected additional S stars south of $\delta = -25°$ and with V magnitudes in the same range as that of Henize. The most severe worry about the completeness of the Henize survey comes from the galactic-plane survey of MacConnell (1979), with 189 stars south of $\delta = -25°$ not belonging to the Henize sample. These stars missed by Henize can certainly not be all explained by a large photometric variability or by very small $(V - R)$ colour indices that would push the R magnitudes of MacConnell's stars below Henize's detection threshold ($R = 10.5$). MacConnell notes that "better plate scale and slightly higher dispersion, larger aperture and excellent optics of the Curtis Schmidt telescope, improved emulsions and variability of some stars are all contributing factors. These will permit one to note stars having weaker ZrO enhancement that would otherwise be the case" (MacConnell 1979). The better plate scale is probably the leading factor that enabled MacConnell to recognise S spectra in crowded regions of the galactic plane.

Fig. 15 shows a comparison of the Henize and MacConnell samples in the region covered by both surveys ($\delta < -25°$ and $|b| < 15°$). The histograms display the eye

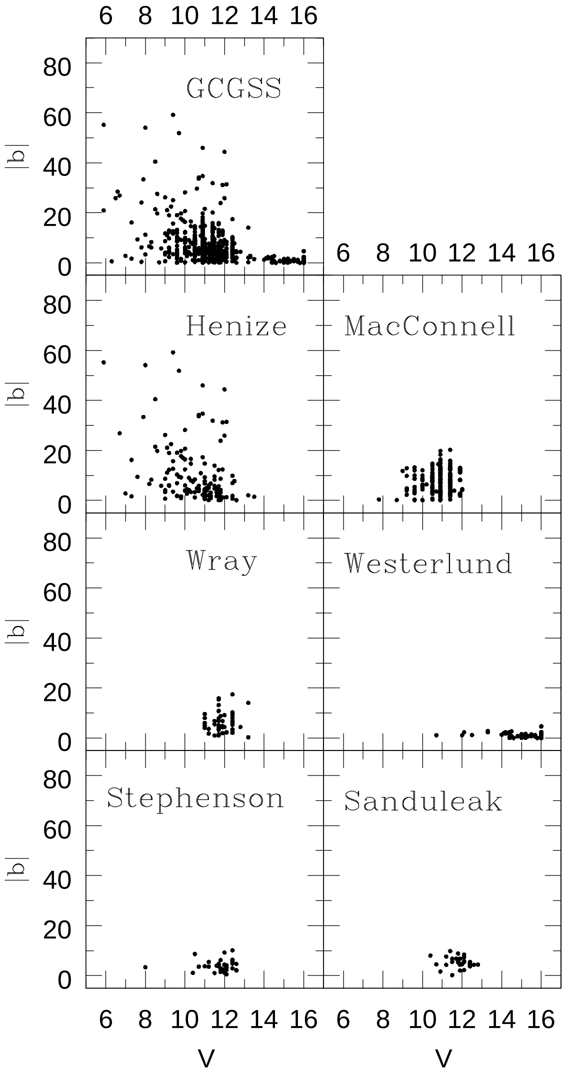

Fig. 14. The galactic latitude distribution for S stars from various surveys, as a function of their V magnitude, as listed in Stephenson (1984). Only the stars south of $\delta = -25°$ and with a V magnitude available in Stephenson (1984) have been plotted. For the McConnell, Wray, Westerlund, Stephenson and Sanduleak surveys [see Stephenson (1984) for detailed references on these surveys], only stars not belonging to the Henize survey are plotted

estimates of the strength of ZrO and TiO bands (as found on K. Henize's unpublished notes, kindly communicated to us by V. Henize). This comparison is meaningful because Henize and MacConnell used similar plates and used quite the same ZrO and TiO bands, though there might be a small horizontal shift between the scale of MacConnell and that of Henize (there are no common stars with TiO and ZrO indices available in the two surveys, that would allow to fix a reference point). Most of the stars missed by Henize have large TiO indices and small ZrO indices. On the top of each bin in Fig.15, the ratio in-

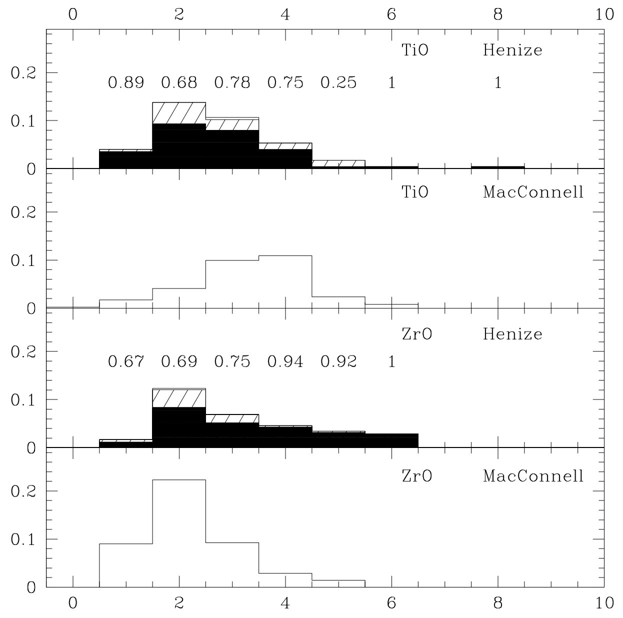

Fig. 15. Comparison of the TiO and ZrO band-strength indices for S stars from the Henize and the MacConnell (1979) surveys. Since Henize surveyed all declinations $\delta < -25°$, and MacConnell virtually all galactic latitudes $|b| < 15°$, only the stars matching both criteria have been plotted. Henize stars are assigned to the extrinsic (hatched) or intrinsic (black) groups according to the classification established in Sect. 6.4.2

trinsic/total is indicated for the Henize stars. Assuming that the same fractions apply to the corresponding MacConnell bins, MacConnell's sample may be split into its extrinsic and intrinsic components. These numbers have then been added to the corresponding numbers of extrinsic and intrinsic Henize stars, in order to yield the extrinsic/intrinsic frequency in the total (Henize + MacConnell) sample. If the above method is applied on the TiO histograms, the extrinsic/intrinsic frequency remains unchanged. This can be understood from the fact that the bins contributing mostly in MacConnell's sample contain similar proportions of extrinsic/intrinsic stars. When considering the ZrO histograms, the extrinsic frequency is increased by a few percents in the (Henize + MacConnell) sample. This results from the fact that MacConnell's sample contains mainly weak ZrO stars which tend to have a higher extrinsic frequency.

In any case these changes turn out to be much less important than the uncertainties from various other sources (see Sect. 9.2) affecting the frequencies derived for the sole Henize sample.

The Wray survey (Wray 1966), based on deeper plates, represents another important source of S stars not retained by Henize, although they were available to him (Wray, priv. comm.). However, including these objects found on such deeper plates covering only the galactic plane would clearly have biased the low galactic latitudes (where most intrinsic stars are found) towards fainter magnitudes.

10. Conclusion

Because a systematic study of a well-defined sample of S stars covering all galactic latitudes and separating intrinsic S stars from their extrinsic analogs was still lacking, the Henize sample of S stars (205 S stars south of $\delta = -25°$ and brighter than $R = 10.5$) has been studied. Radial-velocity data, $UBVJHKL$ and IRAS photometry, as well as low- and high-resolution spectroscopy have been analysed. Given the large number of observational parameters, multivariate classification seemed the best suited method to perform a homogeneous classification. The clustering algorithm used in this paper indeed leads to well-defined stellar groups and is efficient in separating extrinsic from intrinsic S stars, even for the "uncomplete" stars (i.e., that have missing parameters).

The binarity of extrinsic S stars is clearly apparent from their radial-velocity standard-deviation distribution, whereas intrinsic S stars are mostly single, evolved stars with pulsating envelopes.

Neither the extrinsic nor the intrinsic S stars of the Henize sample exhibit any clear concentration along the galactic arms, a conclusion already reached by Yorka & Wing (1979); however these authors did not distinguish extrinsic from intrinsic stars.

Despite uncertainties concerning the absolute magnitudes of S stars and the sampling distances, intrinsic S stars have been shown to be much more concentrated towards the galactic plane than extrinsic S stars. Trying to reconcile their galactic scale heights leads to a clearly implausible luminosity difference. The retained exponential scale heights are 200 ± 100 pc and 600 ± 100 pc for intrinsic and extrinsic S stars, respectively. The frequency of extrinsic stars among S stars probably lies around 40%, but values as low as 30% and as high as 70% cannot be excluded given the large remaining uncertainties.

Acknowledgements. All the observers who contributed to this program through CORAVEL or photometric data are warmly acknowledged. SVE wishes to thank the Geneva Observatory for a four-month stay in 1996, P. Rousseeuw for stimulating discussions about clustering and for a careful and fruitful reading of Sect. 6, I. Glass for kindly providing information on SAAO photometry, and Vance Henize for having sent his late father's unpublished star lists and working notes. SVE was supported by a *F.R.I.A.* PhD fellowship. A.J. is Research Associate, *Fonds National de la Recherche Scientifique* (Belgium). This research has made use of the Simbad database, operated at CDS, Strasbourg, France

References

Abia C., Wallerstein G., 1998, MNRAS 293, 89

Ake T. B., 1979, ApJ 234, 538

Arkhipova V. P., Noskova R. I., 1985, Sov. Astron. Lett. 11, 297

Arnould M., 1991, in G. Michaud, A. Tutukov (eds.), Evolution of stars: the photospheric abundance connection (IAU Symp. 145), Kluwer, Dordrecht, 287

Baranne A., Mayor M., Poncet J. L., 1979, Vistas in Astronomy 23, 279

Barbier M., Petit H., Mayor M., Mennessier M. O., 1988, A&AS 72, 463

Busso M., Gallino R., Lambert D. L., Raiteri C. M., Smith V. V., 1992, ApJ 399, 218

Cardelli J. A., Clayton G. C., Mathis J. S., 1989, ApJ 345, 245

Catchpole R. M., Feast M. W., 1971, MNRAS 154, 197

Catchpole R. M., Feast M. W., 1985, in M. Jaschek, P. C. Keenan (eds.), Cool Stars with Excesses of Heavy Elements, Reidel, Dordrecht, 113

Chen P. S., Kwok S., 1993, ApJ 416, 769

Gillet D., Burki G., Crowe R. A., 1989, A&A 225, 445

Gilmore G., Reid N., 1983, MNRAS 202, 1025

Grenon M., 1978, Ph.D. thesis, Observatoire de Genève

Groenewegen M. A. T., 1993, A&A 271, 180

Henize K., 1960, AJ 65, 491

Henize K., 1965, unpublished

Hron J., 1993, in R. Weinberger, A. Acker (eds.), Planetary Nebulae (IAU Symp. 155), Kluwer, Dordrecht, p. 327

Iben, Jr I., Renzini A., 1983, ARA&A 21, 271

Jorissen A., 1997, in J. Mikolajewska (ed.), Physical Processes in Symbiotic Binaries and Related Systems, Publ. Copernicus Foundation for Polish Astron., Warsaw, 135

Jorissen A., Frayer D. T., Johnson H. R., Mayor M., Smith V. V., 1993, A&A 271, 463

Jorissen A., Hennen O., Mayor M., Bruch A., Sterken C., 1995, A&A 301, 707

Jorissen A., Van Eck S., Mayor M., Udry S., 1998, A&A 332, 877

Jura M., 1994, ApJ 422, 102

Jura M., Kleinmann S. G., 1992a, ApJS 83, 329

Jura M., Kleinmann S. G., 1992b, ApJS 79, 105

Kaufman L., Rousseeuw P. J., 1990, Finding groups in data: an introduction to cluster analysis, Wiley series in probability and statistics, A Wiley-Interscience publication, John Wiley & Sons, Inc., New York

Keenan P. C., 1950, AJ 55, 172

Keenan P. C., 1954, ApJ 120, 484

Keenan P. C., Boeshaar P. C., 1980, ApJS 43, 379

Keenan P. C., McNeil R. C., 1976, An Atlas of Spectra of the Cooler Stars, Ohio State University Press, Columbus

Kerschbaum F., Hron J., 1992, A&A 263, 97

Little-Marenin I. R., Little S. J., 1979, AJ 84, 1374

Little S. J., Little-Marenin I. R., Bauer W. H., 1987, AJ 94, 981

Lloyd Evans T., Catchpole R. M., 1989, MNRAS 237, 219

Lü P. K., 1991, AJ 101, 2229

MacConnell D. J., 1979, A&AS 38, 335

McClure R. D., Woodsworth A. W., 1990, ApJ 352, 709

Morgan W. W., Whitford A. E., Code A. D., 1953, ApJ 118, 318

Mürset U., Schmid H. M., 1999, A&AS 137, 473

Murtagh F., Heck A., 1987, Multivariate Data Analysis, Reidel, Dordrecht

Nakagiri M., Yamashita Y., 1979, Annals of the Tokyo Astronomical Observatory 17, 221

Nassau J. J., 1958, in D. J. K. O'Connell (ed.), Stellar Populations, Ric. Astron. Specola Vaticana, Vol.5, 183

Norris J. E., Green E. M., 1989, ApJ 337, 272

Piccirillo J., 1977, Ph.D. thesis, Indiana University, Bloomington, Indiana, U.S.A.

Piccirillo J., 1980, MNRAS 190, 441

Reid N., Majewski S. R., 1993, ApJ 409, 635

Ridgway S. T., Joyce R. R., White N. M., Wing R. F., 1980, ApJ 235, 126

Rufener F., Nicolet B., 1988, A&A 206, 357

Rybski P., 1972, Ph.D. thesis, Northwestern University, Evanston, Illinois

Scalo J. M., 1976, ApJ 206, 474

Scalo J. M., Ross J. E., 1976, A&A 48, 219

Smith V. V., Lambert D. L., 1990, ApJS 72, 387

Stephenson C. B., 1984, A General Catalogue of Galactic S stars, Second Edition, Publications of the Warner and Swasey Observatory, 3, 1, Columbus

Takayanagi W., 1960, PASJ 12, 314

Udry S., Jorissen A., Mayor M., Van Eck S., 1998, A&AS 131, 25

Van Eck S., Jorissen A., 1999, A&A 345, 127 (Paper I)

Van Eck S., Jorissen A., 2000, A&A, in preparation (Paper IV)

Van Eck S., Jorissen A., Udry S., Mayor M., Pernier B., 1998, A&A 329, 971

Van Eck S., Jorissen A., Udry S. et al., 2000, A&AS, in press (Paper II)

Vanture A. D., Wallerstein G., Brown J. A., Bazan G., 1991, ApJ 381, 278

Vogt N., Moffat A. F. J., 1975, A&A 39, 477

Wallerstein G., 1985, PASP 97, 994

Westerlund B. E., Olander N., 1978, A&AS 32, 401

Wray J. D., 1966, Ph.D. thesis, Northwestern University, Evanston, Illinois

Yorka S. B., Wing R. F., 1979, AJ 84, 1010

Zijlstra A. A., Pottasch S. R., 1991, A&A 243, 478